New Journal of Physics
The open access journal for physics

Prospects for radar detection of cosmic ray air showers with medium-frequency radio waves

M I Bakunov[1,3], A V Maslov[1], A L Novokovskaya[1] and A Kryemadhi[2]

[1] University of Nizhny Novgorod, Nizhny Novgorod 603950, Russia
[2] Department of Mathematical Sciences, Messiah College, Mechanicsburg, PA 17055, USA
E-mail: bakunov@rf.unn.ru

New Journal of Physics **15** (2013) 113027 (12pp)
Received 2 July 2013
Published 13 November 2013
Online at http://www.njp.org/
doi:10.1088/1367-2630/15/11/113027

Abstract. We show that the highly relativistic motion of an extensive air shower allows one to increase the wavelength of the radar signal above its transverse size without giving rise to signal scattering. This increases the efficiency of detection due to an increase in the reflection from the shower and a lower level of sky noise in the frequency range of the reflected signal.

Contents

[3] Author to whom any correspondence should be addressed.

1. Introduction

Extensive air showers (EAS) have been a subject of active research since their first detection in 1938 [1]. EAS are created by cosmic-ray particles impinging on the Earth's atmosphere. Accurate measurements of EAS properties may provide valuable information about the origin of cosmic-rays and our universe.

Traditional ways to measure the characteristics of EAS include counting the shower particles at the ground level, measuring fluorescent light from the excited nitrogen in the atmosphere, detecting the Cherenkov emission in the optical range or radio-emission of geosynchrotron nature from the shower particles [2–4]. An alternative radar concept of EAS detection was proposed more than 70 years ago [5] and was recently revisited [6]. In this concept, a ground-based radio transmitter illuminates the ionization trail left behind EAS and a ground-based detector receives the scattered signal. However, no experimental results of EAS detection using radars have been obtained up to now and therefore, the idea of detecting EAS using radars still remains unconfirmed. Nevertheless, due to potential merits of covering a large detection area and operating with 100% duty cycle [7] the radar concept of EAS detection continues to attract the attention of researchers. For example, the Telescope Array Radar (TARA) project is currently carried out with a 40 kW transmitter broadcasting at 54.1 MHz in conjunction with the telescope array observatory of fluorescence telescopes to confirm the radar detection via time coincidence [8, 9] (www.telescopearray.org/tara/).

In our recent paper [10], we reexamined the radar concept of EAS detection. We showed that the relativistic motion of the EAS front and non-stationarity of the plasma created behind the front are crucial factors that determine the frequency, angle of propagation and amplitude of the reflected signal. We also estimated the feasibility of the concept using the radar signal at 10 MHz. The corresponding wavelength of the signal (30 m) is much smaller than the typical diameter of the EAS disc (∼200 m at a height of 4 km [11]). Using this fact the return signal was calculated under the approximation of an infinitely wide ionization front, i.e. the plane-front approximation.

In this paper, we extend the analysis of the radar detection scheme to the lower frequencies, namely, to the medium frequency (MF) range (300 kHz–3 MHz). This is motivated by the following predictions of the theory developed in [10]. First, reducing the frequency of the incident wave should lead to an increase in the reflection from the ionization front (see figure 4(a) and equation (11) in [10]). Second, the frequency of the reflected signal should simultaneously decrease, for example, the reduction of the incident frequency from 10 to 1 MHz should decrease the reflected frequency from approximately 30 to 3 GHz for typical EAS relativistic factors and angles of incidence (see equation (3) in [10]). At 3 GHz (ultra-high frequency (UHF) band) the level of sky and receiver noise is much lower than at 30 GHz [12, 13].

The wavelengths that correspond to the MF range (100 m–1 km) become comparable to or even larger than the size of the EAS disc. For a stationary disc, this would lead to the scattering of the incident plane wave in all directions, rather than to the reflection in a specific direction. This would lead to the breakup of the plane-wave approximation under which the frequency and the amplitude of the reflected wave was calculated in [10]. The scattering would reduce drastically the power of the signal arriving at the receiver. This limitation was anticipated in [10]. However, as we show in this paper, relativistic effects that lead to the frequency transformation of the reflected and transmitted waves make the plane-front approximation valid even for the

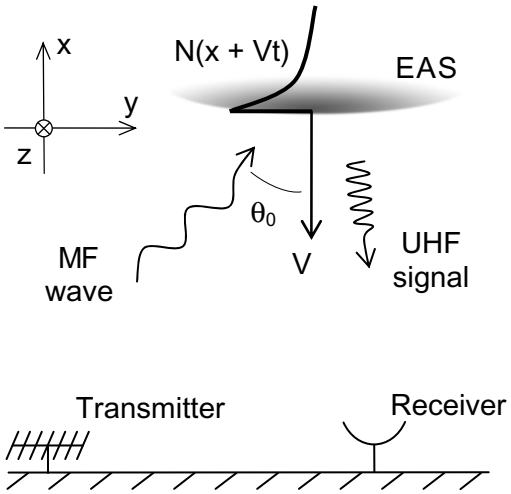

Figure 1. Radar detection of EAS. A MF wave from the ground-based transmitter is obliquely incident on the relativistically moving EAS disc. The reflected Doppler-shifted UHF signal is detected by the receiving antenna. $N(x + Vt)$ is the plasma density profile in the plane-front approximation.

MF range. The validity of this approximation allows one to predict within a relatively simple physical model such properties of the reflected beam as its frequency and amplitude as well as its high directionality. Using lower radar frequencies can therefore be a possible route for more reliable EAS detection.

The paper is organized in the following way. Section 2 outlines the principle of detecting EAS using radars and a physical model for its description. Section 3 introduces main equations and their numerical solution for the reflection from a plasma with finite lifetime. It also provides a justification for neglecting the plasma decay for the values of EAS and radar parameters of interest. This allows one to obtain an analytical solution for the reflected signal described in section 4. Section 5 gives estimates for the feasibility of using MF range for EAS detection. The practicality of the radar detection technique is discussed in section 6 and the conclusions are presented in section 7.

2. The principle of radar detection of extensive air showers (EAS) and its physical model

We consider the geometry of radar detection of a relativistic EAS proposed in [10] and shown in figure 1. A ground-based radio-transmitter illuminates a disc-like EAS created in the atmosphere. The front edge of the disc is an ionization front at which free electrons and ions are created. The front of the disc is moving vertically toward the ground, which is a common situation for the EAS created by ultra-high energy cosmic ray protons. The velocity of the disc V is close to the speed of light c so that the relativistic factor $\gamma_0 = (1 - \beta^2)^{-1/2} \gg 1$ where $\beta = V/c$. The radar signal is assumed to be incident under an angle θ_0 and has frequency 1 MHz (MF range). The reflected signal from the ionization front is received by a ground-based antenna as a Doppler-shifted UHF signal. Our treatment refers specifically to the case when the EAS moves perpendicularly to the ground. The reflection of a wave from an EAS moving at any other angle with respect to the ground can be obtained by specifying the corresponding angle θ_0 between the direction of EAS motion and the incident wave.

The wavelength of the incident wave (300 m) exceeds the diameter of the plasma disc (∼200 m) and therefore it may seem that the assumption of an infinitely large disc used in [10] cannot be used to calculate the characteristics of the reflected wave. However, this is not the case for a highly relativistic disc. In the reference frame of the disc, the wavelength of the incident wave turns out to be much smaller than the diameter of the disc due to the large values of $\gamma_0 \gg 1$. For example, for $\gamma_0 = 30$, the wavelength of the incident wave in the reference frame of the disc is only $5 - 10$ m (depending on the angle of incidence θ_0) and the wave is incident under an angle $\sim\theta_0/\gamma_0$, i.e. almost normally. The assumption of an infinitely wide disc turns out well justified even in this case. We, additionally, assume that the plasma density N in EAS is independent of the transverse coordinates y, z while theoretical estimates predict a decreasing plasma density with the distance from the EAS center [6]. An accurate assessment of the effects of radial plasma inhomogeneity within the EAS disc requires a separate consideration. However, even when the scale of the radial inhomogeneity is smaller than the incident wavelength in the reference frame of the disc one can expect that the waves scattered by the inhomogeneous disc will experience strong relativistic beaming (headlight effect) in the normal to the disc direction. Due to this effect, the radial inhomogeneity of the plasma will actually affect only the amplitude of the reflected signal. While we cannot account for the radial inhomogeneity rigorously, we use in our following calculations the plasma densities intermediate between the core and periphery of the EAS disc. Thus, we take the plasma density in the following form:

$$N(x + Vt) = N_0 \, \mathrm{e}^{-(\mu/V)(x+Vt)} \Theta(x + Vt), \tag{1}$$

where N_0 is the density of the plasma created at the front, μ is the rate of plasma decay and $\Theta(x + Vt)$ is the Heavyside step function. The plasma itself is immobile in the reference frame of the Earth and only its density profile moves according to equation (1). The collision rate in the plasma is ν.

3. Reflection from EAS with finite lifetime

We take a plane electromagnetic wave incident on the plasma with the moving density profile (1). We limit our treatment to transverse electric (TE)-polarization since transverse magnetic (TM)-polarization gives smaller reflection due to the excitation of Langmuir waves [14]. The electric field of the incident wave has the following form:

$$\mathbf{E}_i(x, y, t) = \hat{\mathbf{z}} E_0 \exp(\mathrm{i}\omega_0 t - \mathrm{i}g_0 x - \mathrm{i}h_0 y), \tag{2}$$

where ω_0 is the frequency of the wave ($\omega_0/(2\pi) = 1$ MHz), $g_0 = (\omega_0/c)n\cos\theta_0$ and $h_0 = (\omega_0/c)n\sin\theta_0$ are the normal and tangential wavevector components, respectively; n is the refractive index of the atmosphere. Although n is very close to unity for radio waves (e.g. $n = 1.0001$ at 10 km altitude [15]), including n may be essential for the correct calculation of the return signal in the ultrarelativistic case ($\gamma_0 \gg 1$).

Phase continuity at the moving front (at $x = -Vt$) gives the frequency ω_r and the angle of propagation θ_r for the reflected wave [14, 16]:

$$f_\mathrm{r} = \omega_\mathrm{r}/\omega_0 = \gamma^2(1 + 2\beta n\cos\theta_0 + \beta^2 n^2), \tag{3}$$

$$\sin\theta_\mathrm{r} = f_\mathrm{r}^{-1}\sin\theta_0, \tag{4}$$

where the new relativistic factor $\gamma = (1 - \beta^2 n^2)^{-1/2}$ accounts for the refractive index of the atmosphere. In the ultrarelativistic case ($\beta n \approx 1$ or $\gamma \gg 1$) the frequency f_r changes from

Table 1. Typical values for the basic EAS parameters and derived parameters. The parameters f_p and f_ν were evaluated for $\omega_0/(2\pi) = 1$ MHz.

Parameter type	Symbol	Range of values	Units
	N_0	$10^6 - 10^8$	cm^{-3}
Basic	μ^{-1}	$10 - 100$	ns
	ν	$10^{10} - 10^{11}$	s^{-1}
	γ	$10 - 30$	–
	$\omega_p/(2\pi)$	$10 - 100$	MHz
Derived	βn	0.995–0.999	–
	$f_p = \omega_p/\omega_0$	10–100	–
	$f_\nu = \nu/\omega_0$	$10^4/(2\pi) - 10^5/(2\pi)$	–

$(f_r)_{min} = 2\gamma^2$ at $\theta_0 = 90^\circ$ to $(f_r)_{max} = 4\gamma^2$ at $\theta_0 = 0^\circ$, i.e. $f_r \gg 1$ for any θ_0. For example, for $\gamma = 30$ the frequency of the reflected wave $\omega_r/(2\pi)$ increases from 1.8 to 3.6 GHz when θ_0 decreases from 90° to 0°. In the ultrarelativistic case the reflected wave propagates almost normally to the front ($\theta_r \ll 1$).

To find the amplitude of the reflected wave E_r we solve Maxwell's equations and the equation for the current in the time-varying inhomogeneous plasma, see equations (6*a*)–(6*d*) in [10]. In our calculations, we will use EAS parameters existing in the literature [6, 17] which we have summarized in table 1. The plasma density N_0 is taken from the calculations on the basis of the Nishimura–Kamata–Greisen (NKG) approximation for typical altitudes (5–10 km) and primary particle energies ($10^{19} - 10^{21}$ eV) [6]. The plasma lifetime μ^{-1} in air for $N_0 < 10^{12}\,cm^{-3}$ is determined mainly by attachment of electrons to neutral oxygen molecules and was earlier estimated for different altitudes using an air chemistry code [17]. The collision rate ν is dominated by the electron–neutral molecule collision frequency, which depends on the molecule number density and electron temperature at the altitudes of interest [6]. Since there are no reliable data on the EAS relativistic factor γ in the literature, we take it in a wide interval 10–30.

Figure 2 shows the absolute value of the reflection coefficient $|R| = |E_r|/|E_0|$ as a function of the plasma lifetime μ^{-1} for $\gamma = 30$, $\theta_0 = 45^\circ$ and different N_0 and ν. The dependence $|R(\mu^{-1})|$ saturates with μ^{-1} very fast, at $\mu^{-1} \sim 1$ ns. For smaller $\gamma = 10$ saturation is reached slower, at $\mu^{-1} \sim 10$ ns (not shown). It is interesting that in the case considered in [10] for $\omega_0/(2\pi) = 10$ MHz the saturation of $|R(\mu^{-1})|$ took place at the values of μ^{-1} which are about ten times smaller: 0.1 and 1 ns for $\gamma = 30$ and 10, respectively. This will be explained in section 4.

The numerical results for $|R|$ shown in figure 2 prove that for the typical values of μ^{-1} (see table 1) the decay of plasma behind the ionization front does not affect significantly the reflection coefficient for the incident wave. We therefore can solve the problem neglecting plasma decay, i.e. assuming $\mu = 0$.

4. Reflection from EAS with infinite lifetime

Under the condition $\mu = 0$ the moving front leaves behind itself a stationary immobile plasma with density N_0 and collision rate ν. The transmitted waves $\propto \exp(i\omega_t t - ig_t x - ih_0 y)$ satisfy the usual dispersion equation for the transverse waves in the plasma with the plasma frequency

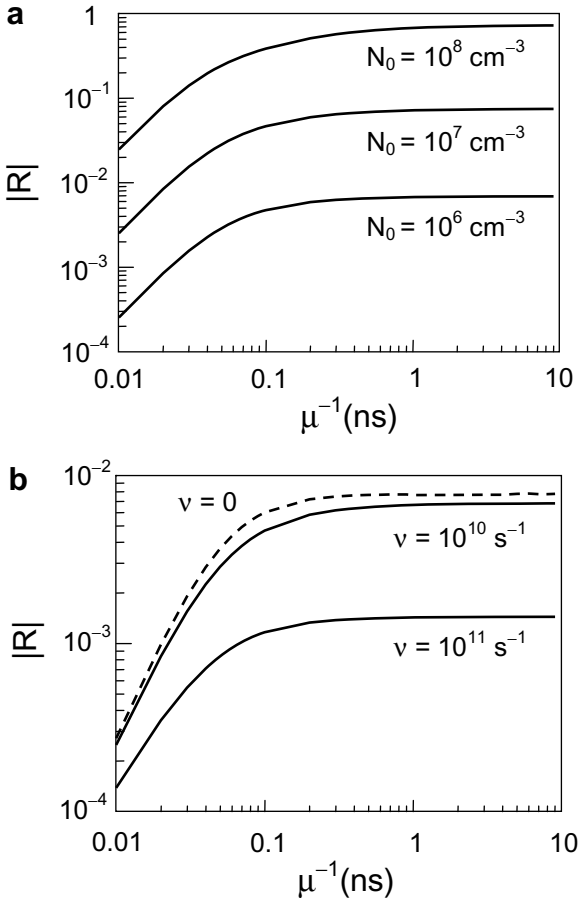

Figure 2. Absolute value of the reflection coefficient $|R|$ as a function of the plasma lifetime μ^{-1} for (a) $\nu = 10^{10}\,\mathrm{s}^{-1}$ and several values of N_0 and for (b) $N_0 = 10^6\,\mathrm{cm}^{-3}$ and several values of ν. The relativistic factor is $\gamma = 30$ and the angle of incidence is $\theta_0 = 45^\circ$.

$\omega_\mathrm{p} = [4\pi \mathrm{e}^2 N_0/(mn^2)]^{1/2}$ and the condition of phase invariance at the boundary [10]. These relations lead to the cubic equation for the frequencies of the transmitted waves [10]

$$\gamma^{-2} f_\mathrm{t}^3 - (2f + \mathrm{i} f_\nu \gamma^{-2}) f_\mathrm{t}^2 + [2(1 + \mathrm{i} f_\nu) f - \gamma^{-2} + \beta^2 n^2 f_\mathrm{p}^2] f_\mathrm{t} - \mathrm{i} f_\nu (2f - \gamma^{-2}) = 0, \tag{5}$$

where $f_\mathrm{t} = \omega_\mathrm{t}/\omega_0$, $f_\nu = \nu/\omega_0$, $f_\mathrm{p} = \omega_\mathrm{p}/\omega_0$ and $f = 1 + \beta n \cos\theta_0$. Only two roots of equation (5) with positive imaginary parts have physical meaning. The third root of equation (5), with a negative imaginary part, should be discarded because it describes an infinitely growing in time solution.

In [10], we obtained approximate solutions of equation (5) in the limit of high values of the collision rate $f_\nu \gg 1$, $f_\nu \gg f_\mathrm{p}^2$ and ultrarelativistic velocity of the ionization front $\gamma \gg 1$. For the case considered here $\omega_0/(2\pi) = 1$ MHz, the inequality $f_\nu \gg f_\mathrm{p}^2$ is not satisfied for all values of ν and ω_p (see table 1). For example, $f_\nu \sim f_\mathrm{p}^2$ for $\nu \sim 10^{10}\,\mathrm{s}^{-1}$ and $\omega_\mathrm{p}/(2\pi) \sim 100$ MHz. We therefore solved equation (5) numerically. Figure 3 shows the dependence of real and imaginary parts of $f_{\mathrm{t}1,2}$ on the parameter f_p. In our case, the parameter f_p lies in the interval $10 \lesssim f_\mathrm{p} \lesssim 100$ while in the case considered in [10] $1 \lesssim f_\mathrm{p} \lesssim 10$.

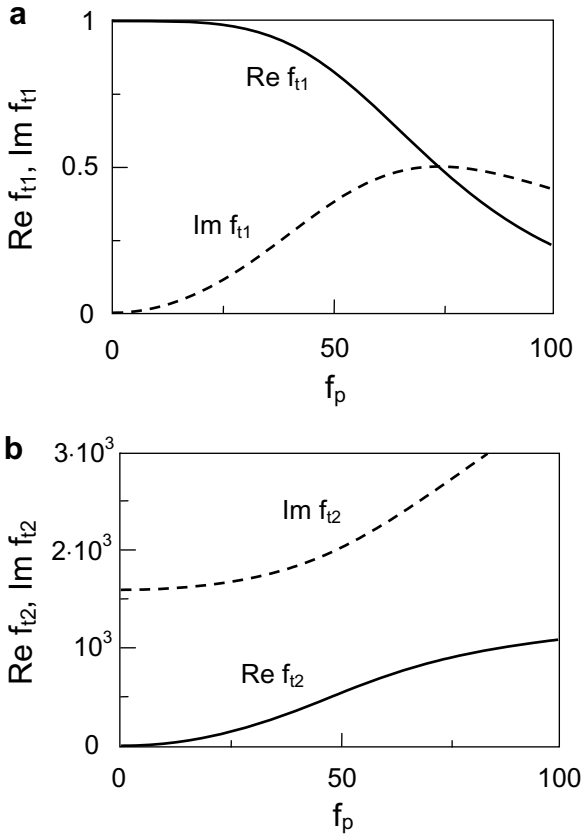

Figure 3. Real and imaginary parts of the frequencies (a) f_{t1} and (b) f_{t2} as functions of f_p for $\gamma = 30$, $\theta = 45^\circ$ and $\nu = 10^{10}\,s^{-1}$.

The wave with Re $f_{t1} < 1$ and Im $f_{t1} < 1$ is the usual transverse wave in highly collisional ($f_\nu \gg 1$) plasma. For $f_p \lesssim 10$ the influence of plasma on this wave is quenched by collisions: the frequency of the wave (Re $f_{t1} \approx 1$ and Im $f_{t1} \approx 0$ in figure 3(a)) and its direction of propagation ($g_t \approx g_0$) are almost the same as for the incident wave. For $f_p > 10$ the plasma affects the wave significantly: Re f_{t1} decreases with increase of f_p while Im f_{t1} increases. The wave with frequency f_{t2} is the generalization of the so-called free-streaming mode to the case of a collisional plasma. The free-streaming mode in a collisionless plasma is a self-consistent distribution of a static magnetic field and dc current [14, 16]. The presence of collisions ($\nu \neq 0$) gives rise to the appearance of a finite electric field for this mode. For $f_p \lesssim 10$ in figure 3(b) the free-streaming mode is described well by the approximate formula $f_{t2} \approx i f_\nu + \gamma^4 f_p^2 f_\nu^{-2}$. For $f_p > 10$, an increase of Im f_{t2} with f_p becomes visible.

The continuity of E_z, B_x and $\partial E_z/\partial x$ at the front gives the reflection coefficient

$$R = \frac{E_r}{E_0} = -f_r \frac{(f_{t1}-1)(f_{t2}-1)}{(f_{t1}-f_r)(f_{t2}-f_r)}. \tag{6}$$

Figure 4(a) shows $|R|$ as a function of f_p for several values of ν, plotted on the basis of equation (6) with $f_{t1,2}$ found from equation (5). The reflection coefficient $|R|$ is higher

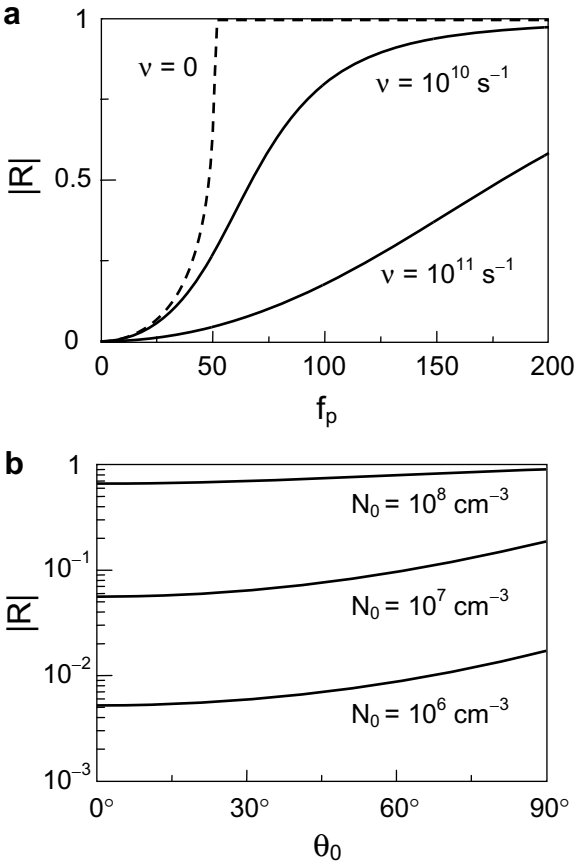

Figure 4. Absolute value of the reflection coefficient $|R|$ as a function of (a) f_p for $\theta_0 = 45^\circ$ and several values of ν and (b) θ_0 for $\nu = 10^{10}\,\mathrm{s}^{-1}$ and several values of N_0. The relativistic factor is $\gamma = 30$.

for smaller collision rates ν, and increases both with f_p and with θ_0 (see figure 4(b)). In general, the reflection coefficient $|R|$ is about two orders of magnitude larger than that for $\omega_0/(2\pi) = 10\,\mathrm{MHz}$ [10]. An increase in γ leads to a decrease in $|R|$, see figure 5.

We now can explain the saturation of reflection with μ^{-1} shown in figure 2. Using Lorentz transformation to the reference frame of the moving front we obtain that the spatial scale of the plasma decay is $L = \gamma V \mu^{-1}$ while the wavelengths of the two transmitted waves are estimated as $\lambda \sim \gamma^{-1}\lambda_0$ with $\lambda_0 = 2\pi c/\omega_0 = 300\,\mathrm{m}$. The plasma inhomogeneity should not cause any reflection of the transmitted wave when $L > \lambda$. This gives the condition for the saturation of R

$$\mu^{-1} \gtrsim \gamma^{-2} 2\pi/\omega_0. \tag{7}$$

For $\omega_0/(2\pi) = 1\,\mathrm{MHz}$, this formula gives $\mu^{-1} \gtrsim 1\,\mathrm{ns}$ for $\gamma = 30$ (which agrees well with the saturation in figure 2) and $\mu^{-1} \gtrsim 10\,\mathrm{ns}$ for $\gamma = 10$. For $\omega_0/(2\pi) = 10\,\mathrm{MHz}$, the corresponding values of μ^{-1} are about ten times smaller and agree well with the result of figure 2 in [10].

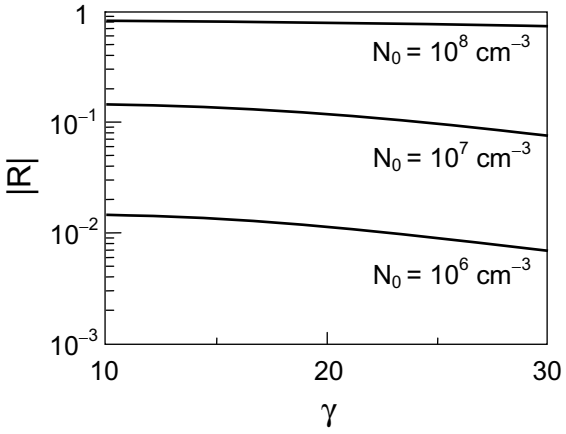

Figure 5. Absolute value of the reflection coefficient $|R|$ as a function of γ for $\nu = 10^{10}\,\mathrm{s}^{-1}$, $\theta_0 = 45^\circ$ and several values of N_0.

5. Estimates for the advantages of using 1 MHz radar frequency

To highlight the advantages of using 1 MHz frequency for radar detection of EAS in comparison with 10 MHz, we compare the power of the reflected wave detected by a ground-based receiver and the levels of noise in the two cases.

Following [10], we assume that the transmitter emits into the upper hemisphere power P_e. For typical diameter of the plasma disc $\sim$200 m and the altitude of EAS $\lesssim 10$ km we can neglect the diffraction spreading of the reflected signal. Unlike [10], here we account for a weak spreading of the reflected beam caused by the curvature of the front (with radius $R_c \sim 7$ km). We arrive at the following formula for the power P_r received by an antenna with an effective area A:

$$P_r = \frac{P_e A |R|^2}{2\pi r^2 (1 + r\cos\theta_0/R_c)^2}, \tag{8}$$

where r is the transmitter–EAS distance and R is the reflection coefficient from the EAS front. For $N_0 = 10^7$ cm^{-3}, $\nu = 10^{10}\,\mathrm{s}^{-1}$, $\gamma = 30$, $\theta_0 = 45^\circ$ and $\omega_0/(2\pi) = 1$ MHz, we obtain $|R| \approx 0.075$ (see figure 4(b)). This value is approximately two orders of magnitude larger than that for $\omega_0/(2\pi) = 10$ MHz under the same values of the other parameters. This means that the received power increases approximately four orders of magnitude when the frequency decreases from 10 to 1 MHz. For example, for the transmitter with $P_e = 200$ kW at 1 MHz located at $r = 10$ km from the ionization front and $A = 3 \times 10^{-3}$ m^2 we obtain from equation (8) $P_r \approx 1.3nW \approx -58.9$ dBm. The frequency of the reflected signal under the chosen values for γ, θ_0 and ω_0 is $\omega_r/(2\pi) \approx 3.07$ GHz, according to equation (3).

One more advantage of radar detection using 1 MHz frequency is the lower level of sky and receiver noise at the frequency of the reflected signal $\omega_r/(2\pi) \approx 3$ GHz. The noise temperature of the sky at this frequency is only a few kelvin, i.e. an order of magnitude smaller than at $\omega_r/(2\pi) \approx 30$ GHz that corresponds to $\omega_0/(2\pi) \approx 10$ MHz [12, 13]. In general, the frequency band 2–15 GHz has the lowest level of sky noise [12, 13]. The noise temperature of the receiver also decreases when moving from 30 to 3 GHz. Estimating the total temperature as $T_N \approx 100$ K,

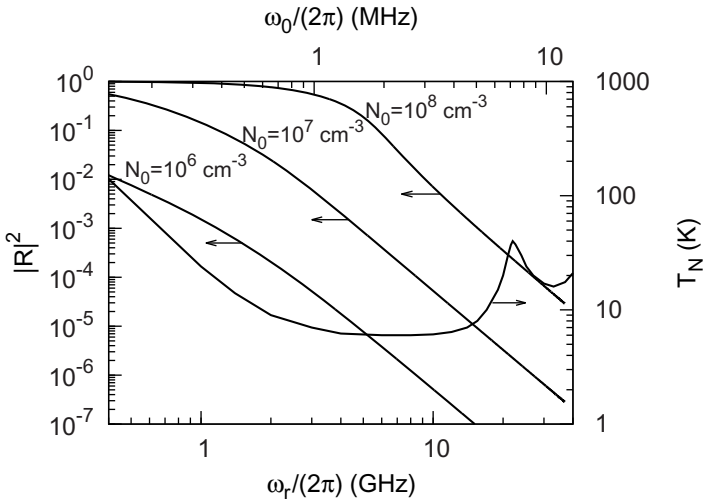

Figure 6. Reflectivity $|R|^2$ and sky noise temperature T_N as functions of the reflected $\omega_r/(2\pi)$ and incident $\omega_0/(2\pi)$ frequencies. Values of N_0 are shown near the corresponding curves. For the chosen parameters ($\gamma = 30$, $\nu = 10^{10}\,\mathrm{s}^{-1}$ and $\theta_0 = 45^\circ$), the frequency of the reflected wave (see equation (3)) is $\omega_r/\omega_0 = 3071.1$. The sky noise temperature was taken from [13] for zero zenith angle of the receiving antenna beam that corresponds to the reflection from a vertically moving EAS.

we obtain the spectral density of noise $p_N = kT_N \approx 1.4 \times 10^{-21}\,\mathrm{W\,Hz^{-1}}$ (k is the Boltzmann constant) which is 1.6 times lower than that at 30 GHz.

Imposing the condition of detectability as a 5 dB ratio of the signal power to the noise power, i.e. $P_r \approx 3 p_N \Delta\omega_r/(2\pi)$, we find the maximal possible bandwidth of the return signal, $\Delta\omega_r/(2\pi) = P_r/(3p_N) \approx 333$ GHz. This bandwidth exceeds significantly the broadening of the reflected spectrum (~500 MHz) dominated by a finite interaction time of the sounding wave with the ionization front [10].

To generalize the analysis of the signal-to-noise ratio (SNR) maximization by a proper choice of the incident frequency, we plotted in figure 6 the reflectivity $|R|^2$ and sky noise temperature T_N as functions of the reflected $\omega_r/(2\pi)$ and incident $\omega_0/(2\pi)$ frequencies. According to figure 6, the lowest sky noise is in the range ~2–15 GHz. For the chosen parameters ($\theta_0 = 45^\circ$ and $\gamma = 30$), the corresponding incident frequencies are in the range 0.65–5 MHz. With reduction of frequencies (<2 GHz), the sky noise grows faster than the reflectivity and thus, the SNR decreases. On the other hand, the high-frequency end of the low noise band corresponds to rather low reflectivities and thus, also gives a small SNR. According to this figure, the incident frequencies slightly below 1 MHz can potentially give the highest SNR. However, the choice of the incident frequency also depends on the angle of incidence θ_0 and relativistic factor γ. For the same γ, the smaller angles θ_0 give a slightly larger frequency upconversion (see equation (3)) and therefore, the incident frequency should be reduced in order to have the reflected frequencies in the low noise band. On the other hand, smaller values of γ (<30) require increasing the incident frequency.

6. Practicality of radar detection

A practical implementation of the proposed scheme for radar detection of EAS requires a continuously emitting MF transmitter of $\gtrsim 200$ kW power with a dipole-like antenna and a receiving station with an array of standard parabolic antennae (0.1–0.6 m diameter), low noise wideband ($\sim$500 MHz bandwidth) preamplifiers and an UHF receiver. To detect vertical or near-vertical EAS, an individual unit of the antenna array may consist of a single vertically oriented parabola. For example, a parabolic antenna of a 0.1 m diameter will cover $\sim$1 sr solid angle (up to $\sim 35^\circ$ zenith angle). To extend the detection to highly slanted EAS, the antenna unit can be made of 4–5 parabolas (depending on their diameter). The area on the ground illuminated by the signal reflected from EAS is defined by the diameter of the EAS disc ($\sim$200 m) and is estimated as $\sim 0.03\,\mathrm{km}^2$. This area can be considered as a coverage area of one antenna unit. For $1\,\mathrm{km}^2$ coverage, 36 antenna units are required (6×6 array). The signal from the antenna units will be passed to the receiver and time tagged using, for example, signals from the global positioning system (GPS). The receiving station will continuously monitor the sky and record events of interest. The correlation with a traditional particle detector array can be done off-line using GPS time tagged events. Moreover, the receiving antenna units of the proposed system can be placed between the detectors of the traditional particle detector array and synchronized with them, similar to the dipole array of the LOPES radio telescope (measuring the geosynchrotron emission from EAS) and KASCADE particle detector array [18]. Total cost for $1\,\mathrm{km}^2$ coverage including the transmitter can be roughly estimated as several hundred thousand dollars.

Since our theory predicts the reflection of the sounding wave in the near-normal direction to a relativistically moving EAS disc, only the air showers with the axes crossing the receiving antenna field can evidently be detected. Thus, the area coverage of the radar detection technique is determined by the area of the receiving antenna field. In this respect, the radar detection is similar to using surface particle detector arrays. For example, to achieve the area coverage of $3000\,\mathrm{km}^2$ of the largest particle detector array (the Pierre Auger Observatory) [2], one needs the receiving antenna field of the equal size. This conclusion is in contrast to the expectation of the TARA project that the radar detectors, like the fluorescence telescopes, can cover a large observation area detecting air showers regardless of their propagation direction [8, 9] (www.telescopearray.org/tara/).

7. Conclusion

To conclude, we propose to use the MF range for radar detection of EAS. Although the wavelength of the radar becomes comparable to the EAS disc diameter, this does not cause the scattering of the incident wave and subsequent reduction of the return signal. The incident wave still experiences diffraction at the edges of the disc but the return signal is dominated by the wave directly reflected by the EAS front. Unlike the case of a stationary scatterer, the relativistically moving disc allows one to use much lower radar frequencies while creating the reflected waves that propagate practically normally to the EAS front. The use of lower frequencies not only increases the reflected signal power due to increased reflection but also moves the frequency of the reflected signal to the frequency range with a lower level of sky and receiver noise.

Our model predicts the frequencies, direction of propagation and amplitudes of the waves reflected from a uniform disc in a wide range of plasma densities. The model emphasizes the relativistic effects. However, the non-uniformity of the plasma density in the transverse

direction [6] brings up additional complications which cannot be assessed with our model and require a separate study.

Acknowledgments

This work was supported in part by RFBR, research project no. 13-02-01423 and Messiah College workload reallocation program.

References

[1] Auger P, Maze R and Grivet-Meyer T 1938 *C. R. Acad. Sci.* **206** 1721
[2] Nagano M and Watson A A 2000 *Rev. Mod. Phys.* **72** 689
[3] Clery D 2004 *Science* **305** 1393
[4] Falcke H, Ape W D, Badea A F, Bähren L, Bekk K, Bercuci A and Bertaina M 2005 *Nature* **435** 313
[5] Blackett P M S and Lovell A C B 1940 *Proc. R. Soc. Lond.* A **177** 183
[6] Gorham P W 2001 *Astropart. Phys.* **15** 177
[7] Ikeda D *et al* 2013 *Proc. 33rd Int. Conf. on Cosmic Ray (Rio de Janeiro)* (www.cbpf.br/∼icrc2013/papers/icrc2013-0360.pdf)
[8] Abou Bakr Othman M *et al* 2011 *Proc. 32nd Int. Conf. on Cosmic Ray (Beijing)* vol 3 pp 340–3
[9] Abou Bakr Othman M *et al* 2013 *Proc. 33rd Int. Conf. on Cosmic Ray (Rio de Janeiro)* (www.cbpf.br/∼icrc2013/papers/icrc2013-1192.pdf)
[10] Bakunov M I, Maslov A V, Novokovskaya A L and Kryemadhi A 2010 *Astropart. Phys.* **33** 335
[11] Scholten O, Werner K and Rusydi F 2008 *Astropart. Phys.* **29** 94
[12] Hogg D C 1959 *J. Appl. Phys.* **30** 1417
[13] Blake L V 1969 *Naval Research Laboratory Report* 5868
[14] Bakunov M I and Maslov A V 1999 *IEEE Trans. Plasma Sci.* **27** 655
[15] Babin S M, Young G S and Carton J A 1997 *J. Appl. Meteor.* **36** 193
[16] Bakunov M I, Maslov A V, Novokovskaya A L, Yugami N and Nishida Y 2002 *Phys. Rev.* E **66** 026404
[17] Vidmar R J 1990 *IEEE Trans. Plasma Sci.* **18** 733
[18] Nigl A, Apel W D, Arteaga J C, Asch T, Auffenberg J, Badea F and Bähren L 2008 *Astron. Astrophys.* **487** 781